Research Article

^{18}F-FDG MicroPET and MRI Targeting Breast Cancer Mouse Model with Designed Synthesis Nanoparticles

Hakimeh Rezaei Aghdam [ID],[1] **Ahmad Bitarafan Rajabi,**[2] **Seyed Esmaeil Sadat Ebrahimi,**[3] **Davood Beiki** [ID],[4] **Khosrou Abdi,**[1] **Seyed Shahaboddin Mousavi Motlagh** [ID],[5] **Banafsheh Kiani Dehkordi,**[6] **Amir Darbandi Azar,**[2] **and Mehdi Shafiee Ardestani** [ID][1]

[1]Department of Radiopharmacy, Faculty of Pharmacy, Tehran University of Medical Sciences, Tehran 1417614411, Iran
[2]Cardiovascular Interventional Research Center, Echocardiography Research Center, Rajaie Cardiovascular, Medical, And Research Center, Iran University of Medical Sciences, Tehran 1449614535, Iran
[3]Department of Medicinal Chemistry, Faculty of Pharmacy, Tehran University of Medical Sciences, Tehran 1417614411, Iran
[4]Research Center for Nuclear Medicine, Tehran University of Medical Sciences, Tehran 1411713135, Iran
[5]Biotechnology Department of Iranian Food and Drug Administration, Ministry of Health, Tehran 1461965381, Iran
[6]Department of Pharmaceutics, Faculty of Pharmacy, Tehran University of Medical Sciences, Tehran 1417614411, Iran

Correspondence should be addressed to Hakimeh Rezaei Aghdam; rezaeihakimeh@yahoo.com
and Mehdi Shafiee Ardestani; shafieeardestani@gmail.com

The first aim of this study was the development of real-time, quantitative, and noninvasive visual observation that necessitates different noninvasive multimodal imaging methods. Second, the design of a high-sensitivity imaging free-ligand green chemistry nanoprobe is a critical diagnosis of breast cancer mouse models. The gadolinium-based nanoparticles as box-Behnken design (BBD) experiment are synthesized. A small biomolecule L-glutamine is attached to its surface nanoparticles as a template. Large surface-area-to-volume ratios of nanoparticles enhance the capacity for interactions with biomolecules and present more sites for conjugation. G. 2-Deoxy-2[^{18}F]fluoro-D-glucose ([^{18}F]F-FDG) is a quantitative and sensitive tracking instrument in Positron Emission Tomography (PET), also applicable for the in vivo and in vitro characterization of L-glutamine SiGdNPs. Optical imaging was done for 4T1 breast cancer tumor-induced mice. ^{18}F-NP uptake values were significantly higher in primary breast cancer and brain tumors than [^{18}F]F-FDG in PET at 30 min, injected (20 μl/g) via the tail vein with about 300 μCi of ^{18}F-FDG loading. After 15 min of the administration of injection (26 μl/g), the first passed the lung intravenously without any injury to the lung showing promising T1-T2 MRI contrast properties. We receive these by application of a variety of imaging modalities, especially microPET and MRI.

1. Introduction

Molecular visualization contributes to a significant perception of biological activities for an exceptional understanding of health and disease. Furthermore, techniques of radioactive imaging have had a remarkable effect on molecular visualization development. Regarding their utilization in biomedical imaging, the characteristics of the desirable nanoparticles (NPs) are biocompatibility (and perhaps bio-degradability), strong imaging signal for a specified technique, and adjustability of surface chemistries, enabling the unification of ligands or bioactive structures. In general, these conditions hold across techniques (magnetic resonance imaging (MRI)), as well as radio, ultrasound, and optical imaging [1, 2]. Probe distribution is a fundamental criterion for imaging applications. Considering pharmacokinetics, the residency time of NP blood and tissue uptake relies on the charge, surface chemistry, and size [3, 4]. The

clearance routes and residency time are prominently identified by the hydrodynamic diameter, although targeting bioactive structures (conjugated antibodies or peptides) may improve absorption to the disease sites.

In response, polysaccharide or polymer coatings commonly change the NP surfaces, thereby decreasing the identification by active and passive clearance mechanisms, increasing circulation time and blood residency, and achieving more uptake at the points of interest. In addition, serum proteins rapidly opsonize the hydrophobic and highly charged particles. This process increases the diameter and improves the recognition by the reticuloendothelial system [5, 6].

Regarding the NPs, as a quantitative and sensitive instrument for tracking, Positron Emission Tomography (PET) is applicable for the characterization of NPs in vivo. Recent developments have occurred incorporating radio metals directly into or onto the NPs for radiolabeling methods which are ligand-free. Signal generation is of critical use in more than one imaging technique to benefit from the potency of each method, specifically for diagnostic and disease monitoring applications. The NP radiolabeling with positron-emitters is equally diverse to that of the single-photon emitting radionuclides. When selecting a PET isotope, considerations such as stability, chemical functionality, and nanostructure composition are significant. Generally, the label selection is based on investigated biological mechanisms and the NP residency time in vivo [7]. In a radiolabeling view, covalent binding commonly utilizes ^{11}C and ^{18}F-FDG or the halogens [124]I and [76]Br labeling directly onto the NP surface or to a spacer subsequently connected to NPs [8, 9]. After implementing essential chemical alterations, ^{18}F-FDG, this can be possibly established by direct binding to the NPs [10].

Nonetheless, issues related to organic solvent, low pH, and high temperature required for radiolabeling may inhibit widespread adoption. Stable coordination chemistry is a prerequisite for carefully employing probes that are altered by PET radiometals in vivo.

Furthermore, a two-step process is often used to obtain chelation so that the chelators are initially conjugated onto the NP surface and radiolabeled subsequently.

Dodecane tetraacetic acid (DOTA) has been utilized for labeling NPs since it can bind different metals stably; moreover, reactive DOTA is available commercially [11]. Kim has tethered ^{18}F onto mesoporous silicon NPs (MSN) using 100-150 nm particle size. The ^{18}F-MSN revealed a solid and constant tumor signal in PET-CT imaging after intravenous injection (IV) into mice carrying subcutaneous U87MG cancer predisposition. However, the mice given free ^{18}F had remarkably less tumor absorption with the renal excretion ability of ^{18}F activity [12].

MRI does not employ any ionizing radiation compared to CT imaging; accordingly, it can be regarded as a safer imaging approach. GdIII-based contrast agents for MRI are utilized in approximately 30% of MRI examinations [13]. Although the FDA-approved contrast agents are among the safest drugs on the market, their core (GdIII ion) has a 50% lethal dose (LD50 around 0.1-0.2 mmol kg^{-1}). There-

fore, for medical diagnostic applications, GdIII ions must be chelated by ligands to prevent the metal ion from being released. All chelators currently employed in the contrast agents clinically approved for MRI are octadentate ligands based either on the open-chain ligand diethylenetriaminepentaacetic acid (DTPA) or the macrocyclic ligand DOTA. Most reported responsive and bifunctional ligands are also derivatives of these two chelators [14–16].

Ligands fulfill two leading roles in GdIII-based contrast agents for MRI, namely, maximizing relaxivity and minimizing dissociation. Many GdIII-based agents have been developed in which the GdIII complex is covalently linked to a high-molecular-weight scaffold with free amino groups on the surface [17]. The synthesis involves functionalizing amino groups with an amine-reactive bifunctional ligand [18], followed by complexation with GdIII ions [19]. Relaxation enhancement only occurs where the target receptor is present, thereby improving target-to-background ratios. In general, the concept of receptor-induced magnetization enhancement is based on reversible binding. Typical polyaminopolycarboxylate-based monohydrated GdIII complexes have longer optimal water residence lifetimes (TM around 200 ns). Since the interaction between the LnIII ions and the bound water is predominant, the water exchange rate is influenced by the electron deficiency around the lanthanide ions. In addition, negatively charged carboxylates tend to increase water exchange rates compared to neutral coordinating groups [20]. The main goal of the targeted contrast agents is to supply the target site with a large payload of paramagnetic centers. Moreover, recent research suggests that GdIII deposition can occur in the brain and bones of patients with normal kidney function who received multiple injections of GdIII contrast agents; however, the medical consequences of these depositions are not yet clear [21].

The utilization of ^{18}F-FDG and PET obtained global approval as an effective instrument to detect cancers with high rates of glycolysis. It is highly recognized that a level of glucose metabolism (Warburg effect) correlated with modifications in gene expression that is alternatively tumor-driven [22]. Nevertheless, despite the firm assurance of ^{18}F-FDG-PET to detect and monitor tumor metabolism, a great portion of malignant tumors are not ^{18}F-FDG-positive and can be missed in an ^{18}F-FDG-PET scan. As a result, it is critical to develop additional metabolic tracers, especially for low-^{18}F-FDG-uptake cancers. Previously conducted studies suggest that metabolic reprogramming may lead to some malignancies modifying their energy source from glucose to glutamine.

Glucose and glutamine are two principal nutrients utilized by cancer cells to increase and survive. Many cancers demonstrate modified glucose metabolism, which accounts are in vivo PET imaging with ^{18}F-FDG [23].

2. Materials and Methods

2.1. For Materials and Instruments.
This includes Gd-nanoparticle synthesis as box-Behnken design (BBD), experiment, preparation of conjugation with L-glutamine, gadolinium leaching test, in vitro characterizations of

nanoparticles, and in vitro apoptosis/necrosis assay (see Supplementary Materials).

2.2. Equipment for PET and MR Imaging

2.2.1. Xtrim PET Scanner.
The Xtrim preclinical high-resolution pet scanner (PNP Co, Tehran, Iran) consists of 10 block detectors based on cerium-doped lutetium-yttrium oxyorthosilicate (LYSO: Ce) crystals arranged in the polygonal full-ring structure. Each detector block consists of a 24×24 crystal array coupled to a 12×12 SiPM array. The size of the detector block is 52×52 mm^2 with a 50.3×50.3 mm^2 active area. Each block consists of a 24×24 LYSO: Ce crystal array with a $2 \times 2 \times 10$ mm^3 pixel size. The pixels are wrapped with a 0.5 m $BaSO_4$ reflector, which results in a 2.1 mm pixel pitch. The system uses SensL ARRAYS-30035-144P which is a 12×12 array of C-series SiPM pixels (SensL DS 2014).

2.3. MRI Scanner.
Tesla 3 Siemens Prisma was used for MR imaging with Scanner Coils: 1H Rat Coil (with rat holder) in mouse models.

3. Results

3.1. In Vitro and In Vivo.
Characterization was introduced in detail in Supplementary Materials (Figures S1–S4, Tables S1–S4, and Equation S1). Briefly, in vitro characterizations of SiNPs, SiGdNPs, and Gln-SiGdNPs (FTIR, fluorescence spectra, UV/vis, LC-MASS, zeta potential, DLS, SLS, ICP-MS, FESEM, MAP, TEM, and EDS) were performed for each particle as needed. Cell cytotoxicity and viability, apoptosis/necrosis assay (flow cytometry), gadolinium leaching test, cellular uptake, and biodistribution studies (in vivo cellular uptake of Gln-SiGdNPs) are done to assess the prepared nanoparticles (see Supplementary Materials file).

3.2. In Vivo Imaging

3.2.1. Positron Emission Tomography Imaging.
The more enduring isotopes are suitable for checking the rapid systems' constant operations over months or years. However, the transistor isotopes are beneficial for cross-validating the PET systems, dose calibrator, and gamma counter using the data obtained from imaging investigations. The long-lasting phantoms can be achieved typically and commercially from the scanner manufacturer. The fillable phantom employs centrifuge tubes utilizing isotopes. They are easily procurable (F-18) or uniform objects as cylindrically fillable (soda bottles).

Considering mice, a 20-28 ml plastic liquid scintillation vial is an easily affordable choice readily attainable with a diameter rather larger than that of the majority of mice that show tumor to background ratio of 2.17, brain to background ratio of 3.9, and tumor to brain ratio of 0.556 (60 minutes after injection).

After matching the obtained data with data processing in control mice, tumor to the background, brain to the background, and tumor to brain ratios were obtained at 1.42,

1.10, and 1.20, respectively (60 minutes after injection) (Table 1 and Figure 1). Matching with data processing in control mice shows tumor to background ratio of 1.42, brain to background ratio of 1.10, and tumor to brain ratio of 1.20, 60 minutes after injection.

Since 18FDG and Gln-SiGdNPs attach by covalent and hydrogen bonds, Scheme 1.

3.3. Protocol: The Time of PET Imaging per Bed Position Carried Out at Four Minutes

3.3.1. Quantitative Data, Materials and Methods, Small-Animal PET Imaging, and Image Analysis.
A microPET scanner (Xtrim PET) was used to obtain the small-animal PET scans. Under general anesthesia, the animals were each injected ($20 \mu l/g$) via the tail vein with about $300 \mu Ci$ of the ^{18}F-FDG loading. For each small animal (female balb/c 4T1 mammary tumor ($n = 3$, 18-20 g)) PET scan, 3D regions of interest were drawn manually around the tumor and the brain. After background correction, the brain tumor to the background uptake ratios were estimated as follows: (region counts per voxel)/(background counts per voxel).

Thin-layer chromatography (TLC) used acetone/methanol (1 : 1) solvent as a mobile phase. Six μl of samples was spotted on the beginning of the Whatman paper strips (1.2 cm × 10 cm) and strips inserted in solvents. A gamma well counter for each segment determined the radioactivity of segments of the strips. In acetone/methanol, ^{18}F-FDG was not moving with the solvent (Rf = 0). The L-Gln-SiGdNPs moved with the solvent (Rf = 0.5), while ^{18}F-FDG-NPs (Rf = 1).

3.4. MR Imaging.
MRI noninvasive medical imaging technology is used by researchers or physicians for numerous purposes, such as the diagnosis, staging, and monitoring of the disease progression, the evaluation of the reactions to treatments, and medication discovery. For the creation of detailed images of the body structures, an MRI scan utilizes a gradient magnetic field, a powerful and static magnetic field, processing devices, and radiofrequency pulses. This imaging technology is used to examine any body parts (the brain and spinal cord).

3.4.1. Sagittal Localizer.
A 2-D gradient-echo sequence covering the entire phantom should be utilized. The criteria that are recommended include flip angle (FA) = 20°, TE/TR = 5 /15 ms, field of view (FOV) = 3 cm, readout bandwidth = 130 Hz/pixel, matrix size = 128 × 128, slide thickness = 1 mm, and the number of signal averages (NEX) = 1.

3.4.2. T1-Weighted (T1W) Axial Images.
A 2-D spin-echo sequence should be utilized. The parameters included readout bandwidth = 130 Hz/pixel, TE/TR = 650/1500 ms, slide thickness = 1 mm, matrix size = 128 × 128, field of view (FOV) = 3 cm, and number of signal averages (NEX) = 1. It is worth mentioning that images should be obtained through the center of the phantom considering three orthogonal planes (coronal, axial, and sagittal).

TABLE 1: Target/nontarget ratios in microPET imaging.

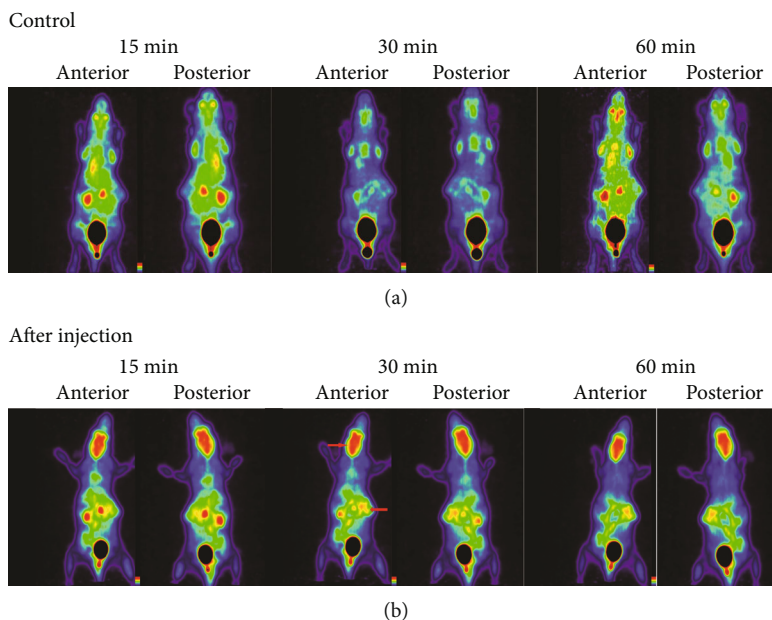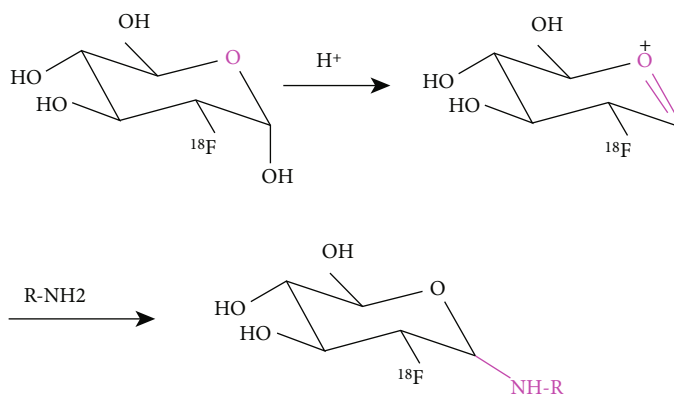| MicroPET			
Mouse model		BBR (brain background ratio)	TBR (tumor background ratio)
Test	60 min	2.17 ± 0.01	3.9 ± 0.01
Control	60 min	1.42 ± 0.02	1.1 ± 0.01

(a)

(b)

FIGURE 1: PET imaging: (a) control before Gln-SiGdNP injection; (b) after injection.

SCHEME 1: ^{18}F-FDG is combined and Gln-SiGdNPs are attached by a covalent and hydrogen bond.

3.5. T2-Weighted Axial Images. A 2-D spin-echo sequence utilizes the same criteria and slice position as the T1W images, except for TE/TR = 75/1000 ms. The SNR (phantom signal-to-noise ratio) is calculated using the formula:

$$SNR = 0.655 * mean - \qquad (1)$$

Since noise is distributed normally around zero, the correction factor (0.655) is utilized. Display of a magnitude image (no negative values) and Fourier transformation of the raw data lead to the attainment of skewed-distributed noise multiplied by 0.655 to be corrected. The SNR can be lower because of either an increase in noise or a decrease in signal.

Before the injection of NPs, the control images were divided into two groups (low and high concentration). After 15 min of the administration of injection (26 μl/g) into the tail (female balb/c 4T1 mammary tumor ($n = 3$, 18-20 g)), the mice were assigned into groups of low (50 μl/ml) and high (100 μl/ml) concentrations (Figures 2(a)–2(i)).
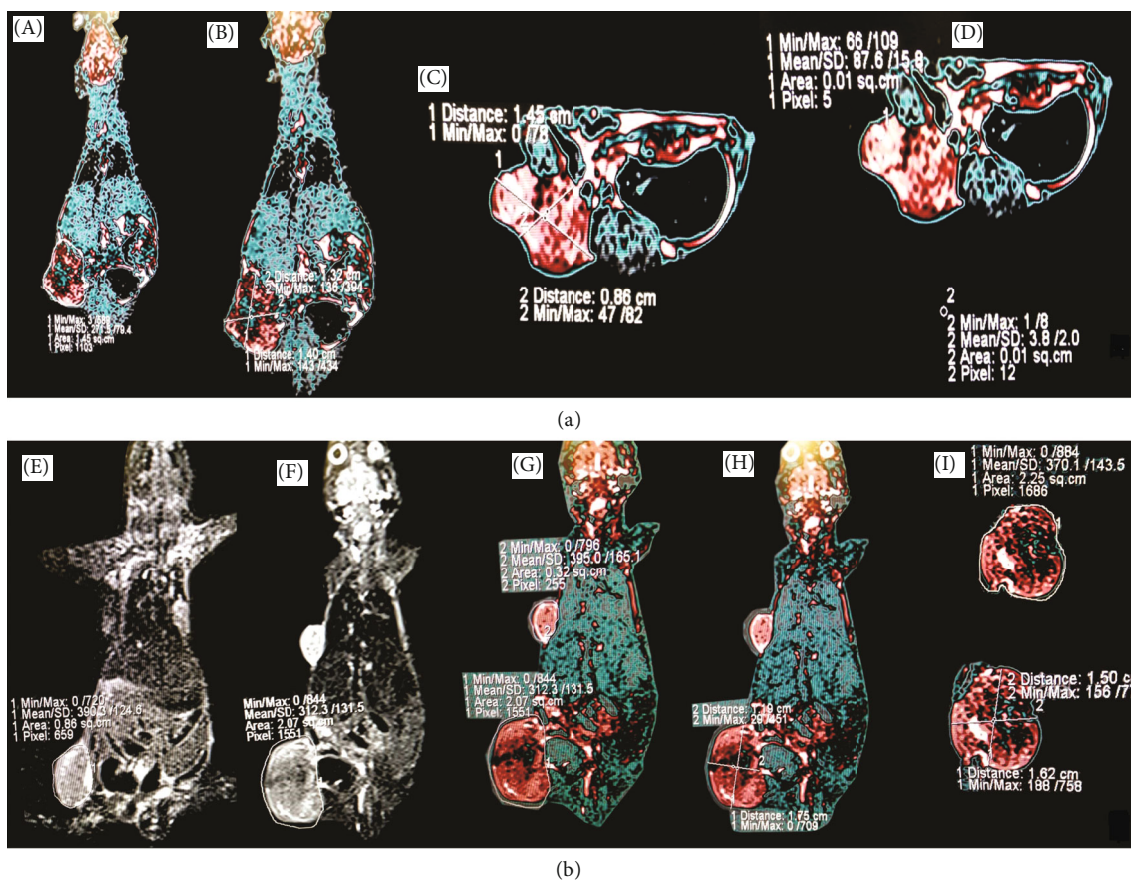
(a)

(b)

FIGURE 2: MR imaging: (a) low concentration injection of Gln-SiGdNPs; (b) high concentration injection of Gln-SiGdNPs.

TABLE 2: Target/nontarget ratios in MR imaging.

MRI	Tumor/ stomach	Tumor/ lung	Ratios Tumor/ liver	% conjugated NPs in tumor
T1	0.833 ± 0.06	1 ± 0.01	0.5 ± 0.02	50 ± 0.01
T2	2 ± 0.05	1 ± 0.01	0.833 ± 0.01	43.8 ± 0.01

Furthermore, in two T1W images, the ratios of tumor pixel on a liver pixel are 0.75 and 1.75, respectively.

In the high concentration group, the T1W coronal image was in the field of (1) tumor, (2) stomach, and (3) liver. Moreover, the ratios of tumor pixels on the stomach and liver are 0.833 and 2 pixels, respectively. The FOV phase is 50% which means the percent of the FOV base (Table 2).

In the high concentration group (Figure 3(b)) is the T2W coronal image in the field of (1) tumor, (2) stomach, and (3) liver.

The ratios of the tumor pixel on the stomach and the liver are 1 and 1 pixel, respectively. In the field of view image, the ratios of tumor pixels on the stomach, liver, and lung (4) are 2, 0.833, and 1 pixel, respectively. The FOV phase is 43.8% which is the percent of the FOV base. The ratio of the target (tumor) to the nontarget is significant (Table 2).

The presence of hydroxyl and amide groups on NPs caused high hydrophilic properties, followed by easy and rapid exertion and low toxic side effects on nerve cells. These nonionic NPs have lower realized histamine properties. However, the first passed the lung intravenously without any injury to the lung (Figures 3(a) and 3(b)), showing promising T1-T2 MRI contrast properties. For nonionic properties, there is low protein binding and rapid exertion by kidneys.

The Gd-incorporated mesoporous silica was rendered to a versatile new class of MRI contrast agents by the observed high r1 and r2 values, nanosize, and easy derivatization of silica.

The influence of APTES was explored, and regarding the trisodium citrate mole ratios (8.4 : 1), 60.98% yield was achieved. In addition, the mole ratios of the two reactants achieved reaction time and reaction temperature by alteration. The produced gadolinium-doped silica NPs using the Stöber process is an ideal material because of the monodispersity [24–26]. Accordingly, gadolinium silicon NPs are formed in larger sizes. It should be mentioned that they are more stable due to a smaller surface-to-volume ratio compared to small-size nanocrystals. Furthermore, to produce any desirable amount of SiGdNPs, the process can be scaled up by utilizing reactants with an appropriately larger amount. A dialysis bag was employed for purifying the prepared solution at the end of the preparation. It was then

(a)
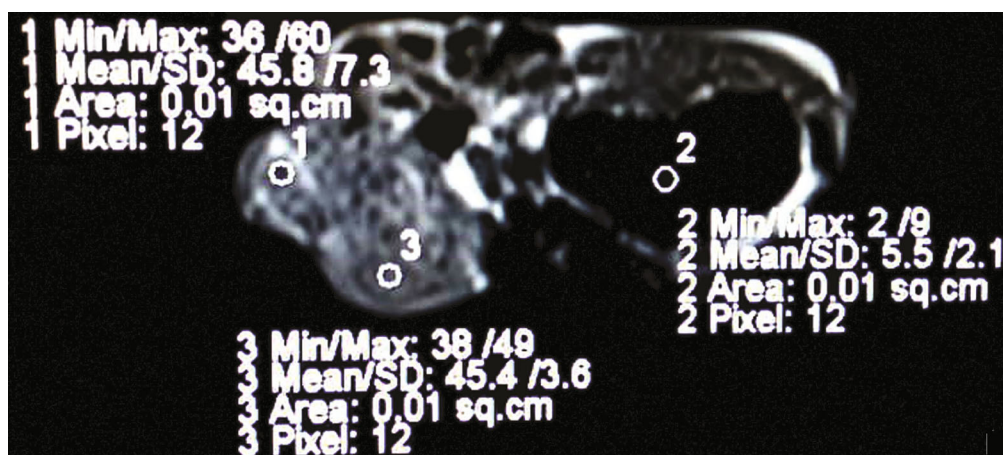
(b)

FIGURE 3: MR imaging in high concentration injection of Gln-SiGdNPs: (a) T1 imaging; (b) T2 imaging.

collected and lyophilized into a white or light yellow solid and stored at 4°C for use.

3.6. Optical Imaging Systems Are Moderately Plain. It differs from other imaging methods of headache. Also, signals in optical imaging turned into images (Figure 4(a) (control), Figure 4(b) (15 minutes after injection), and Figure 4(c) (isolated organs)).

4. Discussion

These NPs react in both reactions, namely, chelates and NPs. Also, these findings confirmed that this novel complex conjugation could be an effective cancer imaging agent for molecular biology and molecular nuclear imaging applications. These multifunctional silica NPs with an ability such as adjustable incorporation ability, tunable surface chemistry, several functions, and versatile structure can regard as a diagnosis probe for cancer. Silica is a multifunctional matrix, which can act as a connecting matrix or coating materials to integrate different imaging techniques.

The biocompatibility of these NPs could be increased by coating silica on the other functional NPs. Moreover, if needed, the metabolism, in vivo biodistribution, and excretion may be real-time monitored. At first, the combination of several diagnosis techniques into one nanoparticle leads

to a synergistic therapeutic effect over one single therapeutic technique to induce more efficient diagnosis outcomes. Moreover, when designing the NPs, the researchers should consider different pharmacokinetic conditions of imaging modalities and therapeutic agents.

The surface of cylindrical silica NPs is doped with GdIII ions (white or light yellow crystals of SiGdNPs) conjugated with biomolecule L-glutamine (solid white powder), the covalent attachment of L-glutamine chains to the surface of SiGdNPs, the corresponding amide. The characteristic carbonyl stretching vibration at $1681 \, cm^{-1}$ due to the carboxylate moiety shifted down to $1617 \, cm^{-1}$ upon reaction with Gd^{+3} and consequent conversion of the COOH group into an amide. The particles were inherently negatively charged due to the presence of carboxyl terminus residues. Conjugation of glutamine to particles greatly reduced their charges, with average size (136.5296 nm), molecular weight (Z-average: $3.29 \pm 1.09 \, kD$), and -29.3 surface charge zeta potential. The obtained optimal nanoparticles are ready for the next steps of imaging in this research.

There is greater solubility in water and the presence of amine and hydroxyl groups for more hydrophilic properties, thereby excreting them sooner and faster; however, their toxic effects are lower on neurons. These NPs have enough where the stability study of the conjugated NPs showed just a bit of the gadolinium ions (<5) without inconsiderable
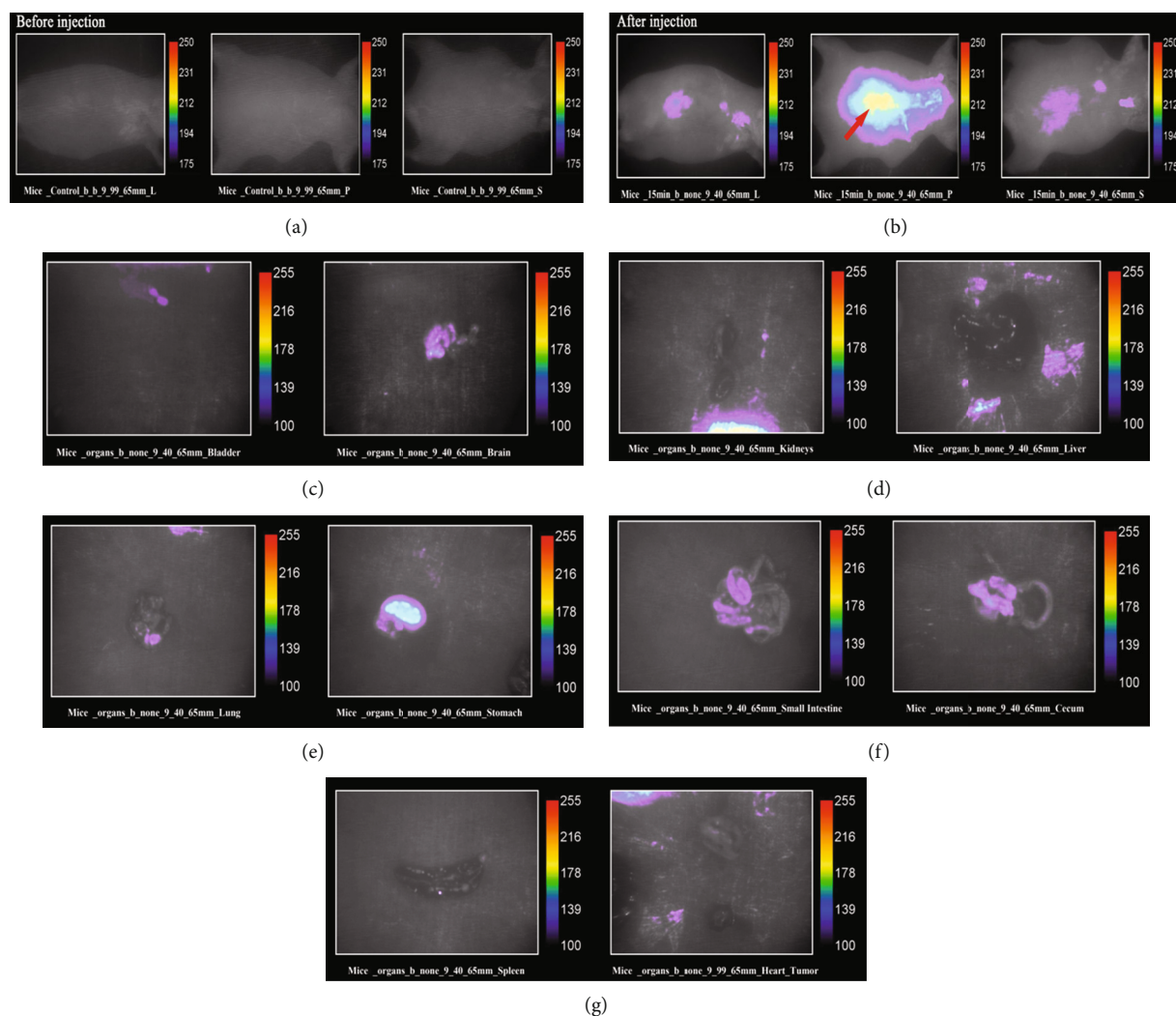
(a)

(b)

(c)

(d)

(e)

(f)

(g)

FIGURE 4: Optical imaging: (a) control, (b) 15 minutes after injection of Gln-SiGdNPs, and (c) isolated organs.

leaching. This leaching is because of partial degradation that occurs on the polysiloxane matrix level with the hydrolysis of the Si-O-Si bonds [24, 27].

In cancer therapy, silica-based multimodal imaging and theranostics have experienced remarkable developments. The multifunctionality and diversity of the silica-based NPs lead to a bright way to invent cooperative treatments or use several imaging modalities simultaneously to guide nanomedicine delivery. It is expected that silica-based NPs lead to a more effective personalized cancer therapy. However, it takes a long way to translate the multifunctional silica-based NPs into the clinical market since it necessitates the accumulation of sufficient evidence to prove their efficacy and safety. There have been many attempts to understand the real capacity of molecular imaging techniques to deliver a series of advances. Accordingly, communities mentioned earlier reach common goals and issues affecting their research outcomes. In addition, it is of utmost importance to educate researchers to devise kinetically stable probe systems without a need for possessing any acute/chronic toxicity problems or giving rise to unwanted off-target accu-

mulation/irradiation effects. Furthermore, it is necessary to define what is possible in terms of detection limits, time scales, and targets.

Particularly, translation continues to offer a tremendous challenge to the community. It means that better mechanisms must be developed to promote effective communication between primary researchers and end-users. Moreover, early diagnosis is the means to treat diseases effectively and cost-effectively. There are limiting financial models that restrict the utilization and development of diagnostics. These limitations are augmented by the need to use intellectual resources effectively across a range of areas. It is hoped that at the beginning of the next phase of a broader dialogue, industry and academics can work together more effectively to address these important challenges in the chemistry of molecular imaging. The parameters for successful clinical translation and validation of diagnostic applications are now becoming much better understood. It is an exciting time of progress for these agents as the advances in chemical synthesis continue to yield new structures with precisely defined biochemical features, and emerging analytical

techniques continue to shed new light on nuanced and context-dependent nano-bio interactions. Furthermore, our ability to exploit and treat human diseases using synthetic NPs will continue to grow as rapidly as the field has expanded over the past several years.

We trial Gln-SiGdNPs only [18]FDG-labeled, 4T1 cells, balb/c mice with several other radionuclides, cancer cells, and greater animals than balb/c mice.

5. Conclusions

This study reported a gadolinium-based surface unfunctionalization (chelated free) technique to develop L-glutamine-conjugated SiGdNPs for 4T1 breast cancer tumor targeting in vivo and finally obtained improved diagnostic effects, compared to the functionalized SiGdNPs by chelator. It is very difficult and may be different among patients to know how to meet the needs of each functional modality, such as in vivo imaging. Furthermore, the biocompatibility of imaging agents can be increased using a silica matrix; however, the potential toxicity of these agents should be paid enough attention to after exposure or leakage, especially their long-lasting toxicity in vivo. It is an exciting time of progress for these agents as their potential is closer to being realized with translation into the clinic.

Abbreviations

Gd: Gadolinium
APTES: (3-Aminopropyl) triethoxysilane
UV: Ultraviolet spectrum
FTIR: Fourier transform infrared spectroscopy
FL: Fluorescence spectroscopy
TEM: Transmission electron microscopy
FESEM: Field emission scanning electron microscopy
SLS: Static light scattering
LC-MS: Liquid chromatography spectrometry
DLS: Dynamic light scattering
EDS: Energy-dispersive X-ray spectroscopy
ICP-MS: Inductively coupled plasma mass spectrometry
OI: Optical imaging
Gln: Glutamine
SiNPs: Silicon nanoparticles
SiGdNPs: Gadolinium-based silicon nanoparticles
Gln-SiGdNPs: Glutamine-conjugated gadolinium-based silicon nanoparticles
XTT: 2,3-Bis-(2-methoxy-4-nitro-5-sulfophenyl)-2H-tetrazolium-5-carboxanilide
PET: Positron emission tomography
MRI: Magnetic resonance imaging.

Data Availability

The data used to support the findings of this study are available from the corresponding authors upon request.

Conflicts of Interest

The authors declare no conflict of interest.

Supplementary Materials

Addition experimental details include Figures S1–S4, Tables S1–S4, and Equation S1. (*Supplementary Materials*)

References

[1] V. C. Pierre and M. J. Allen, "Contrast agents for MRI: experimental methods," in *2nd, Royal Society of Chemistry, United Kingdom by CPI Group (UK) Ltd*, R. B. M. Schasfoort, Ed., Croydon, CR0 4YY, UK, 2017.

[2] X. Shi, C. Cao, Z. Zhang, J. Tian, and Z. Hu, "Radiopharmaceutical and Eu^{3+} doped gadolinium oxide nanoparticles mediated triple-excited fluorescence imaging and image-guided surgery," *Journal of Nanbiotechnology*, vol. 19, no. 1, 2021.

[3] P. Kolhar, A. C. Anselmo, V. Gupta, K. Pant, B. Prabhakarpandian, and E. Ruoslahti, "Using shape effects to target antibody-coated nanoparticles to lung and brain endothelium," *Proceedings of the National Academy of Sciences*, vol. 110, no. 26, pp. 10753–10758, 2013.

[4] A. Banerjee, J. Qi, R. Gogoi, J. Wong, and S. Mitragotri, "Role of nanoparticle size, shape and surface chemistry in oral drug delivery," *Journal of Controlled Release*, vol. 238, no. 176–185, pp. 176–185, 2016.

[5] M. Longmire, P. L. Choyke, and H. Kobayashi, "Clearance properties of nano-sized particles and molecules as imaging agents considerations and caveats," *Nanomedicine (London, England)*, vol. 3, no. 5, pp. 703–717, 2008.

[6] S. Behzadi, V. Serpooshan, W. Tao et al., "Cellular uptake of nanoparticles: journey inside the cell," *Chemical Society Reviews*, vol. 46, no. 14, pp. 4218–4244, 2017.

[7] E. Phillips, O. Penate-Medina, P. B. Zanzonico, R. D. Carvajal, P. Mohan, and Y. Ye, "Clinical translation of an ultrasmall inorganic optical-PET imaging nanoparticle probe," *Science*

Translational Medicine, vol. 6, no. 260, p. 260ra149-260ra149, 2014.

[8] K. Stockhofe, J. M. Postema, H. Schieferstein, and T. L. Ross, "Radiolabeling of nanoparticles and polymers for PET imaging," *Pharmaceuticals*, vol. 7, no. 4, pp. 392–418, 2014.

[9] F. Schulz, I. Lokteva, W. J. Park, and F. Lehmkühler, "Recent notable approaches to study self-assembly of nanoparticles with X-ray scattering and electron microscopy," *Particle & Particle Systems Characterization*, vol. 38, no. 9, article 2100087, 2021.

[10] M. Jauregui-Osoro, P. A. Williamson, A. Gloria et al., "Biocompatible inorganic nanoparticles for [¹⁸F]-fluoride binding with applications in PET imaging," *Dalton Transactions*, vol. 40, no. 23, pp. 6226–6237, 2011.

[11] T. J. Wadas, E. H. Wong, G. R. Weisman, and C. J. Anderson, "Coordinating radiometals of copper, gallium, indium, yttrium, and zirconium for PET and SPECT imaging of disease," *Chemical Reviews*, vol. 110, no. 5, pp. 2858–2902, 2010.

[12] A. Almutairi, R. Rossin, M. Shokeen et al., "Biodegradable dendritic positron-emitting nanoprobes for the noninvasive imaging of angiogenesis," *Proceedings of the National Academy of Sciences*, vol. 106, no. 3, pp. 685–690, 2009.

[13] S. Aime and P. Caravan, "Biodistribution of gadolinium-based contrast agents, including gadolinium deposition," *Journal of Magnetic Resonance Imaging: An Official Journal of the International Society for Magnetic Resonance in Medicine*, vol. 30, no. 6, pp. 1259–1267, 2009.

[14] E. G. Moore, A. P. S. Samuel, and K. N. Raymond, "From antenna to assay: lessons learned in lanthanide luminescence," *Accounts of Chemical Research*, vol. 42, no. 4, pp. 542–552, 2009.

[15] S. Cotton, *Lanthanide and Actinide Chemistry*, John Wiley & Sons, Wiley Chichester UK, 2013.

[16] Q. N. Do, J. S. Ratnakar, Z. Kovács et al., *General synthetic and physical methods, in Contrast Agents for MRI: Experimental Methods*, The Royal Society of Chemistry UK, 2017.

[17] M. R. Longmire, M. Ogawa, P. L. Choyke, and H. Kobayashi, "Dendrimers as high relaxivity MR contrast agents," *NanoBiotechnology*, vol. 6, no. 2, pp. 155–162, 2014.

[18] C. Bernhard, M. Moreau, D. Henry et al., "DOTAGA–anhydride: a valuable building block for the preparation of DOTA-like chelating agents," *Chemistry - A European Journal*, vol. 18, no. 25, pp. 7834–7841, 2012.

[19] J. Tang, Y. Sheng, H. Hu, and Y. Shen, "Macromolecular MRI contrast agents: structures, properties and applications," *Progress in Polymer Science*, vol. 38, no. 3–4, pp. 462–502, 2013.

[20] S. Dumas, V. Jacques, W.-C. Sun, J. S. Troughton, J. T. Welch, and J. M. Chasse, "High relaxivity magnetic resonance imaging contrast agents part 1: impact of single donor atom substitution on relaxivity of serum albumin-bound gadolinium complexes," *Investigative Radiology*, vol. 45, no. 10, pp. 600–612, 2010.

[21] W. H. Koppenol, P. L. Bounds, C. V. Dang, and O. Warburg's, "Otto Warburg's contributions to current concepts of cancer metabolism," *Nature Reviews. Cancer*, vol. 11, no. 5, pp. 325–337, 2011.

[22] J. Ramalho, R. C. Semelka, M. Ramalho, R. H. Nunes, M. AlObaidy, and M. Castillo, "Gadolinium-based contrast agent accumulation and toxicity: an update," *American Journal of Neuroradiology*, vol. 37, no. 7, pp. 1192–1198, 2016.

[23] D. Daye and K. E. Wellen, "Metabolic reprogramming in cancer: unraveling the role of glutamine in tumorigenesis," *Seminars in Cell & Developmental Biology*, vol. 23, no. 4, pp. 362–369, 2012.

[24] Y. Feng, Y. Liu, C. Su, X. Ji, and Z. He, "New fluorescent pH sensor based on label-free silicon nanodots," *Sensors and Actuators B: Chemical*, vol. 203, pp. 795–801, 2014.

[25] S. Li, F. Wang, X. W. He, W. Y. Li, and Y. K. Zhang, "One-pot hydrothermal preparation of gadolinium-doped silicon nanoparticles as a dual-modal probe for multicolor fluorescence and magnetic resonance imaging," *Journal of Materials Chemistry B*, vol. 6, no. 20, pp. 3358–3365, 2018.

[26] Z. Xiaohui, Z. Dongfang, F. Zexuan, H. Zhang, M. Hongju, and M. Yunfei, "One-step hydrothermal synthesis of ultrabright water-soluble silicon nanoparticles for folate-receptor-mediated bioimaging," *Journal of Materials Science*, vol. 54, no. 13, pp. 9707–9717, 2019.

[27] X. Liu, J. Liu, Y. Guan et al., "Establishment of an orthotopic lung cancer model in nude mice and its evaluation by spiral CT," *Journal of Thoracic Disease*, vol. 4, no. 2, pp. 141–145, 2012.